POLYMER SEPARATORS FOR HIGH TEMPERATURE LITHIUM SULFUR BATTERIES

Charles Leroux, Ryan Cruz, Geoff Geise*, and Gary Koenig*
University of Virginia Department of Chemical Engineering

Abstract

Space exploration increasingly relies on energy storage to carry out missions. Improving the energy density and maximum operating temperature of batteries would reduce weight and improve operations. Lithium sulfur (Li-S) batteries may fit this need because of their high theoretical energy density and high thermal stability. However, significant challenges are preventing Li-S batteries from reaching their potential.

Polysulfide shuttling (crossover of polysulfide species from the cathode to the anode) is a common challenge that results in high capacity fade and low battery lifetime. Selective membrane separators, which allow for high lithium ion conductivity but prevent the crossover of polysulfide species, need to be developed. In this work, a cation exchange membrane was developed for use in a model Li-S battery environment. Overall the membrane demonstrated stability in electrolytes used for Li-S batteries and conductvities as high as 0.2 mS/cm. During lithium metal symmetric coin cell cycling, the membrane demonstrated slightly higher conductivies (0.4 mS/cm) and high stability over 100 cycles. Overall, this work highlights the potential for this CEM to be employed in a Li-S battery.

Background

Energy storage is critical to space missions, providing power for satellites, extravehicular activities (EVAs), planetary landers, and rovers.[1] Li-ion batteries have a relatively high energy density, power, and low thermal dissipation, but they exhibit high capacity fade and limited stability at high temperatures.[1,2] Specifically, exploration of the inner planets, like Venus, presents a unique challenge where atmospheric temperatures reach as high as 400 °C. Therefore, to build towards missions like VERITAS, Venus flagship, and Venus in-situ explorer (as described in the LAND: Entry, Decent, or Landing NASA Strategic Framework) battery technology must be improved for operation at elevated temperatures. Even increasing the operating temperature range relative to conventional Li-ion would reduce system level battery weight to improve mission capabilities.

A promising battery chemistry to fit this high temperature application is metal-sulfur, which relies upon a solid metal anode and a sulfur composite cathode, allowing them to operate at elevated temperatures.[3,4] Lithium metal-sulfur (Li-S) batteries have received growing attention due to their high theoretical specific energy density of 2500 Wh/kg and demonstrated cell capacity over 500 Wh/kg.[2,2,4–13] However, several technical challenges have prevented the realization of the Li-S chemistry's performance potential.

One of the most significant challenges is polysulfide shuttling.[2,4–6,8,9,11,13,14] During the charge/discharge process, the reaction with Li at the sulfur cathode occurs through several steps that produce polysulfide species from Li_2S_2 to Li_2S_8 (**Figure 1).**[2,5–9,11–13,15] These polysulfide species readily dissolve in organic electrolytes used in Li-S batteries and crossover into the anode side of the cell.[2,5–14] The crossed-over species will then reduce, causing capacity fade within the cell.[2,4–8,10–14]

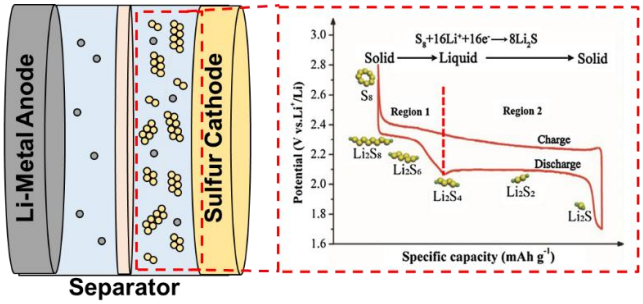

Figure 1: Schematic of a lithium-sulfur battery system outlining the polysulfide species produced during cycling.[5]

Selective separators need to be developed to prevent the cross-over of polysulfide species during the cycling process while allowing for Li^+ conduction to improve long-term performance of Li-S batteries while maintaining reasonable rates of charge/discharge.

The desired properties for membrane separators for Li-S batteries are: high Li^+ conductivity, low polysulfide permeability, and stability in organic solvents and in contact with lithium metal.[4,9,16–18] Our lab has developed a polymer membrane based on a poly(phenylene oxide) (PPO) backbone that leverages phenoxyaniline trisulfonate (POATS) fixed charge groups to enhance interactions with Li^+ (The chemical structure is provided in **Figure 2**).[19,20] PPO is a non-polar, high glass transition temperature (220 °C) polymer. It is stable at reasonably high temperatures and could help build towards a high temperature battery system.[19–23] When functionalized to the PPO backbone, the POATS fixed charges promote transport of lithium ions while limiting interactions with positively charged dissolved polysulfide species enhancing membrane selectivity.[17] In this work, the POATS-PPO membrane will be applied to a model Li-S battery system. The solvent uptake, ionic conductivity, and stability in contact with lithium metal will be evaluated. These properties will help to identify the opportunity for the membrane to function as a separator for Li-S batteries.

Methods

Crosslinked Membrane Synthesis

Br-PPO Synthesis

In procedure that was similar to previous reports,[19–21,24] poly(phenylene oxide) (PPO, SABIC NORYL blend 646) was functionalized via a free radical bromination using the bromine source *N*-bromo-succinimide (NBS, >98% TCI Chemicals) and azobisisobutyronitrile (AIBN, 98% Sigma) initiator.[19,20,24] Two different degrees of bromination (indicated as X or Y in **Figure 2)** were targeted for use as an intermediate for POATS-PPO synthesis (X = 18%, **Figure 2**) or for use as a crosslinker (Y = 85%, **Figure 2**). For each PPO bromination reaction, 6 g of PPO was dissolved in 75 mL of chlorobenzene at room temperature, and then this mixture was placed in an oil bath at 110 °C. Next, 3.3 g and 10.2 g of NBS (for X = 18% and Y = 85 % respectively) and 0.056 g of AIBN per gram of NBS were massed and split evenly into 4 separate vials (containing both NBS and AIBN), and the mixture in each vial was added to the reaction flask (containing the PPO solution) at 15 min intervals over the course of 45 min. After adding all the NBS and AIBN, the reaction was allowed to proceed for an additional 30 min (i.e., the total reaction time was 75 min).

The reaction mixture was then added, all at once, to 750 mL of reagent alcohol (Fisher Chemical), which resulted in precipitation of the Br-PPO. The precipitate was collected via filtration (Cytiva, Whatman 4). The polymer was dried under vacuum at room temperature (22 °C) for 3 h, dissolved in 50 mL of chloroform, and precipitated again using 500

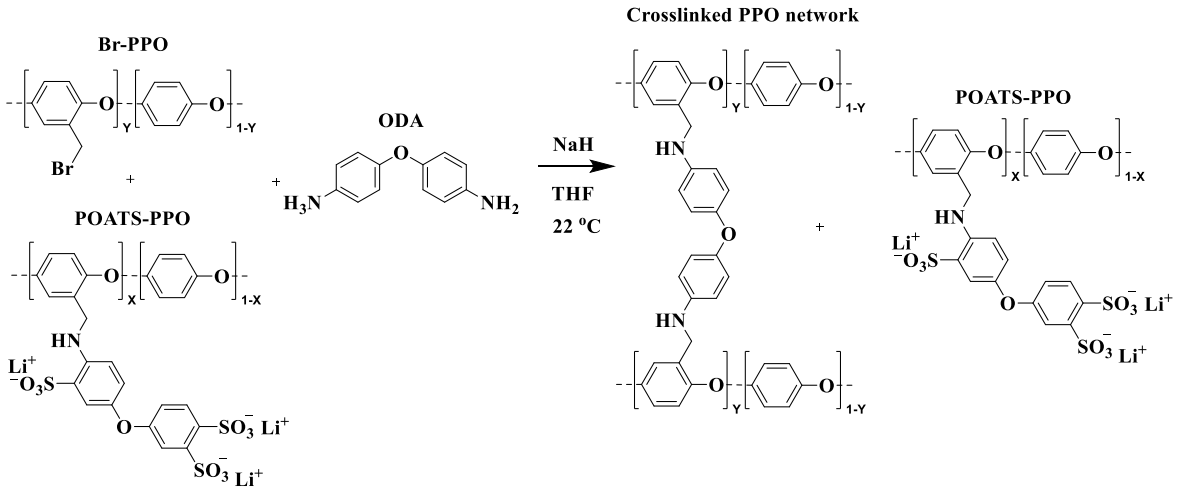

Figure 2: Schematic for crosslinked POATS-PPO membrane synthesis. Br-PPO (Y=85) was used as the crosslinker, and POATS-PPO (X=18) was used as the ion exchange polymer in the membrane. ODA was used as the crosslinker between Br-PPO 85 chains.

mL of reagent alcohol to further purify the target Br-PPO polymer material. The final polymer was collected by filtration and dried under vacuum at room temperature (22 °C) for 24 h.

POATS Synthesis

POATS was synthesized via aromatic sulfonation of 4-phenoxyaniline (Sigma) using a previously reported procedure.[19–21] Briefly, 4 g of 4-phenoxyaniline was dissolved in 30 mL of fuming sulfuric acid (Sigma, 20% as free SO_3), in an ice bath. Once dissolved, the reaction mixture was placed in an oil bath and the temperature was increased to 80 °C over the course of 30 min and held at 80 °C for 2 h. The reaction mixture was then poured over 100 g of ice made from deionized (DI, 18.2 MΩ cm, Direct-Q 3 UV, Millipore) water and then diluted with additional DI water to a total volume of 1 L.

Next, 9 mL of triethylamine (TEA) was added to convert the POATS to the triethylamine counterion form (TEA^+), and ~68 g of calcium carbonate (Sigma) was added subsequently to neutralize the remaining sulfuric acid. The precipitated calcium sulfate was removed by filtration. The collected liquid solution was dried in a rotary evaporator, filtered to remove any remaining calcium sulfate, collected and dried in a convection oven at 80 °C for around 16 h and then under vacuum at room temperature for 24 h.

POATS-PPO Synthesis

POATS-PPO was synthesized using a modified procedure from previous reports,[19–21] to achieve a higher degree of functionalization. To reduce water contamination, all reactants and glassware were dried under vacuum at room temperature (22 °C) for at least 16 h prior to synthesis. First, 0.6 g of Br-PPO was dissolved in a solvent blend containing 4 mL of *N*-methyl pyrrolidone (NMP, Macron) and 4 mL of chlorobenzene (Sigma, 99%) and 2 equivalents (per mol of Br) of POATS and sodium bicarbonate were dissolved (separately from the Br-PPO) in 16 mL of NMP.

The POATS solution was added to a reaction flask and placed in an oil bath at 60 °C. The Br-PPO solution was then added dropwise to the reaction flask. The reaction

was allowed to proceed for 24 h and the reaction mixture was poured into 250 mL of isopropyl alcohol (IPA, VWR) for precipitation of the POATS-PPO polymer. The suspension was centrifuged, and the liquid was decanted. The precipitate was washed with DI water and centrifuged twice to remove excess POATS from the polymer. The solid product was dispersed in reagent alcohol (VWR) and dried under vacuum at room temperature (22 ℃) for at least 16 h.

Membrane Crosslinking

A crosslinked membrane was formed by reacting amine groups from oxydianiline (ODA, Sigma, 97%) with free bromine groups on Br-PPO using a previously reported method (**Figure 2**).[20] For a typical membrane, 0.08 g of POATS-PPO-18 and 0.0167 g of Br-PPO-85 were dissolved separately in 2 mL of dimethyl formamide (DMF, Sigma). The two solutions were combined, briefly stirred, and poured into a 6 cm diameter Teflon mold. The solution in the mold was dried at 80 ℃ in a convection oven for 3 h and subsequently under vacuum at 80 ℃ for 24 h. The nominal dried membrane thickness using this procedure was typically ~65 μm.

After drying, the sulfonate groups on the POATS-PPO membranes were converted into the lithium counter-ion form by soaking the membrane in 0.5 M lithium chloride (LiCl, Sigma) solution for 3 h. The LiCl solution was replaced with fresh LiCl solution, and the membrane was soaked for an additional 3 h. The film was then soaked in DI water for 1 h and subsequently dried under vacuum at 80 ℃ for 24 h.

To form the crosslinked network, a Li^+ counter-ion form POATS-PPO membrane soaked in a solution of 1 mg ODA per mL tetrahydrofuran (THF, Sigma, >99%, 250 ppm BHT inhibitor), where the ODA solution had been contacted with 1 g of 4 Å molecular sieve powder (Sigma) in a glass jar for a minimum of 24 h. The volume of ODA solution was chosen to match the equivalents of ODA amines with the equivalents of bromine on the polymer (e.g., 7.75 mL ODA solution for an 85 mg POATS-PPO-18 / Br-PPO-85 membrane). Crosslinking was then initiated by adding 0.05 g of sodium hydride (60% NaH dispersed in mineral oil, Sigma) and the mixture was allowed to react for 24 h. The reaction was quenched by quickly removing the membrane from the solution and placing it in a glass jar containing 30 mL of de-swelling solution (acetonitrile, (ACN, 99.8% anhydrous, Sigma), ethanol, or DI water). The membrane was left in de-swelling solution for 6 h to allow for the membrane to sufficiently equilibrate, following previous reports.[20] The membrane was subsequently moved to a glass jar containing 30 mL of measurement solvent (triethylene glycol dimethyl ether (TEGDMDE, Sigma), or a blend of dimethoxy ethane (DME, Sigma) and dioxolane (DOL, Sigma)). DME:DOL blends were made in 3:1, 1:3, and 1:1 ratios by volume. The measurement solvent was replaced after 24 h to minimize contamination of de-swelling solvent in the final membranes. Membranes were stored in the measurement solvent until further use.

Structural Characterization

^{1}H Proton Nuclear Magnetic Resonance Spectroscopy

Structural characterization used to make the crosslinked membranes was performed using proton nuclear magnetic resonance spectroscopy (^{1}H proton NMR, Varian 600 MHz). $CDCl_3$ (99.8% deuterated, Sigma) was used as the solvent for Br-PPO and d_6-DMSO (Sigma, 99.9%) was used as the solvent for POATS and POATS-PPO.

Spectra were collected on 10 mg of sample dissolved in 1 mL of deuterated solvent.

Differential Scanning Calorimetry

Differential scanning calorimetry (DSC) was used to determine the glass transition temperature (T_g) of the membranes. A mass of 10 mg of dry membrane was characterized by scanning twice from 50 ºC to 315 ºC at a scan rate of 10 ºC per minute. The first scan was performed to eliminate the thermal history of the polymer and remove excess solvent from the sample. The T_g values were obtained during the second scan using the midpoint between inflection points on the thermogram indicating a glass transition within the polymer.

Physical Characterization

Solvent and Electrolyte Uptake

Solvent uptake (*SU*) was measured by removing the membrane from the measurement solvent, the surface was quickly wiped dry of excess solution and the sample was massed to obtain the solvated mass of the membrane ($m_{solvated}$). Those membranes were then placed in an empty vial under vacuum at 80 ℃ for 24 h and massed again to obtain the dry mass of the membrane (m_{dry}). The solvent uptake of the membrane was then calculated as:

$$SU = \frac{m_{solvated} - m_{dry}}{m_{dry}} * 100\%$$

Ionic Conductivity

The conductivity of the membranes investigated in this work was evaluated via electrochemical impedance spectroscopy (EIS) using a coin cell without active material components. To evaluate different electrolytes, 1M lithium bistrifluoromethane-sulfonylimide (LiTFSI, TCI) was dissolved in TEGDME or one of the DME:DOL mixtures, and the membrane was soaked in the electrolyte solution for at least 24 hours prior to any conductivity measurement. The coin cell was assembled with four stainless steel spacers with a solvated polymer membrane separating the bottom two spacers from the top two spacers. The active area of the cell was around 2 cm^2. A spring was placed on top of the spacers and the cell was clamped in between two stainless steel electrodes for the measurement.

EIS was performed by varying the frequency of the potential oscillations around the open circuit potential of the solution with an amplitude of 10 mV (Biologic SP-300 Potentiostat). The frequency range was 1 MHz to 100 Hz. The membrane resistance was taken as the high frequency intercept of the Nyquist plots obtained using the coin cell. The conductivity was then calculated by using the membrane resistance, thickness (L), and active area (A) as:

$$Conductivity = \frac{L}{A \times R}$$

Li-Metal Symmetric Coin Cell Cycling

Lithium metal symmetric coin cells were assembled by first pressing two 12 mm diameter pieces of lithium metal onto separate (1.6 cm diameter) stainless steel spacers to serve as the anode and cathode of the cell. Each spacer was placed into the button cell casing and separated by either a Celgard porous separator or the POATS-PPO membrane for use in cycling testing. Coin cells were cycled on a MACCOR cycler at a constant current of 0.1 mA for over 100 cycles.

Results and Discussion

Structural Characterization

The degree of bromination of the Br-PPO used to synthesize these membranes was verified first using ^{1}H NMR. Peaks at 2.1 and

6.5 ppm were attributed to the aliphatic and aromatic hydrogens, respectively, of the PPO backbone.[19–21,24] A distinct chemical shift of the aliphatic hydrogens from 2.1 to 4.3 ppm was observed with the addition of bromine to one methyl group of the PPO repeat unit.[19–21,24] The degree of bromination (*DB*) was calculated using the ratio of integrated peaks at 4.3 and 2.1 ppm as:[19–21,24]

$$DB = \frac{2}{1 + \frac{2}{3} \times \frac{Peak\ (2.1\ ppm)}{Peak\ (4.3\ ppm)}} \times 100\%$$

For use as a crosslinker, the *DB* of the Br-PPO was 85 %. Additional Br-PPO was synthesized for use as an intermediate with a *DB* of 18 %. The POATS molecule was allowed to react with the intermediate Br-PPO, leading to a POATS functionalization of 18 %. The conversion of the halogenated polymer to POATS-PPO was verified using ^{1}H NMR. Substitution of the Br groups to POATS resulted in an additional chemical shift from 4.3 ppm to 4.0 ppm. Conversion to POATS-PPO was thus confirmed via disappearance of the peak at 4.3 ppm and the final degree of substitution of the POATS-PPO polymer used in the crosslinked membrane was confirmed via the Equation for *DB*, where the peak area at 4.3 ppm was replaced by the peak area at 4.0 ppm at 18 %.

DSC was used to evaluate the T_g of the membranes used in this study. A significant endothermic peak was observed between 200 ºC and 240 ºC, consistent with the degradation of the sulfonate groups on the polymer.[25,26] The T_g of the PPO used for membrane synthesis was 217 ºC.[27] Because of the decomposition of the membrane occurred below the T_g of the functionalized PPO, the T_g of the membrane could not be evaluated with DSC.[26] For use in high temperature applications, the membrane is stable up to 200 ºC and it does not appear that the T_g will be reached.

Physical Characterization

To control the downstream properties of the crosslinked membranes a de-swelling solvent is used during the crosslinking procedure. The de-swelling solvent causes the polymer chains to collapse after crosslinking helping to control downstream solvent uptake and transport properties.[20] Three different de-swelling solvents were evaluated, and ACN was selected for use in future experiments because it had the lowest uptake of the three solvents evaluated (**Figure 3**). Using ACN as the de-swelling solvent, the solvent uptake of the crosslinked membranes was evaluated in different measurement solvents **(Figure 3)**.

Mixtures of (DME) and (DOL) were used in this work as they are commonly used in

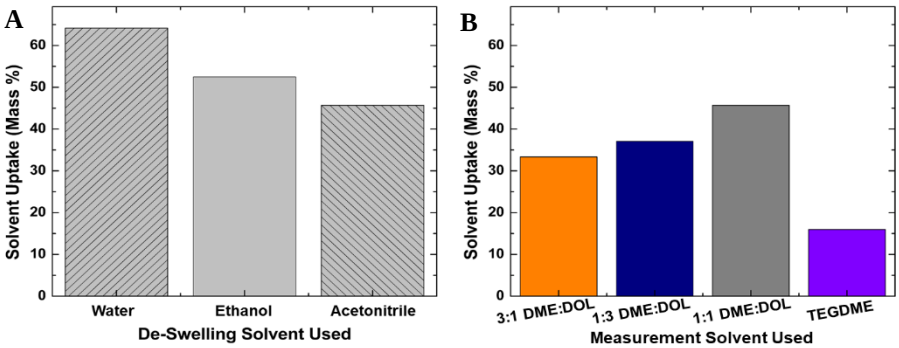

Figure 3: (A) Solvent uptake for POATS-PPO-18 membrane using three different De-Swelling Solvents. (B) Solvent uptake for POATS-PPO-18 membranes using acetonitrile as the de-swelling solvent and different ratios of DME:DOL as well as TEGDME as the measurement solvent.

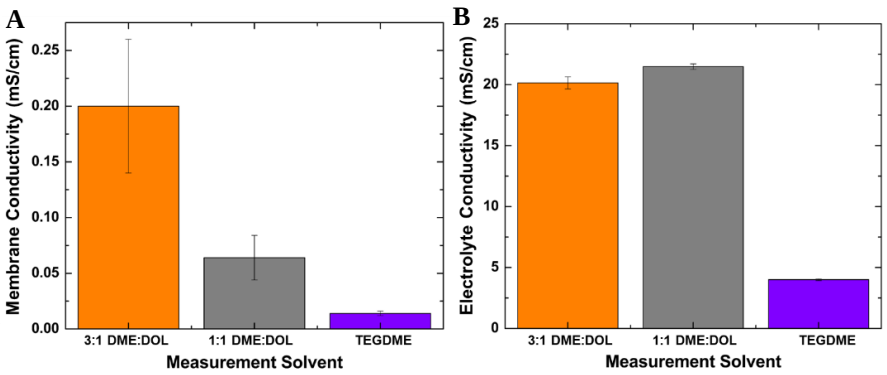

Figure 4: (A) Conductivity of POATS-PPO-18 membranes using ACN as the de-swelling solvent and 1 M LiFSI in different measurement solvents as the electrolyte. (B) Conductivity of 1 M LiTFSI electrolvte in each measurement solvent.

Li-S batteries,[10] and TEGDME is a solvent with similar polarity but can be used at much higher temperatures. TEGDME has the lowest solvent uptake in the POATS-PPO membrane, likely due to the size of the molecule (**Figure 3**). TEGDME is much larger than the other solvent molecules used in this study, so incorporation of TEGDME may be blocked by the polymer chains causing the low solvent uptake. Using different ratios of DME and DOL demonstrates how co-solvent behavior can influence solvent uptake. For the 3:1 and 1:3 DME:DOL mixtures, increasing the DOL content increases the solvent uptake. This could be caused by a size effect, similar to TEGDME, where the smaller DOL molecules are able to solvate the polymer matrix better than the larger DME chains. The 1:1 DME:DOL mixture has a larger solvent uptake than either the 3:1 or 1:3 DME:DOL mixtures indicating that the size of DOL alone is not responsible for the uptake behavior. Co-solvent interactions between DME and DOL may enhance the solvent interactions with the POATS-PPO polymer, leading to a high solvent uptake for the mixture where there are equal parts DME and DOL.

Generally, solvent uptake drives transport properties in dense polymer films. Therefore, it is expected that the conductivity of the solution will increase with increasing electrolyte uptake. The membrane has the lowest electrolyte uptake in the TEGDME solution and the lowest conductivity, which aligns with expectations (**Figure 4**). However, the membrane conductivity is lower in the 1:1 DME:DOL electrolyte than the 3:1 DME:DOL electrolyte, even though the electrolyte conductivities are roughly the same (**Figure 4**) and higher solvent uptake in the 1:1 DME:DOL mixture (**Figure 3).**

The high resistance of the membranes in the 1:1 DME:DOL electrolyte may be caused by a skin layer on the membrane. In commercial CEMs, it has been observed that a thin layer of dense hydrophobic polymer can form along the surface of the membrane.[28] This skin layer may orient itself differently depending on the electrolyte environment.[28] The orientation of the skin layer may be influenced by the amount of DME in the electrolyte, or the co-solvent behavior of the DME:DOL blends.

Li-Metal Symmetric Coin Cell Cycling

To evaluate the stability of the membrane in contact with lithium metal, a symmetric

coin cell was fabricated using lithium metal as the anode and cathode separated by a polymer membrane. As a control, a Celgard porous membrane was used which has demonstrated high stability and low resistance in contact with lithium metal. 1 M LiTFSI in 3:1 DME:DOL electrolyte was used for coin cell cycling because it allows for the highest membrane conductivity of the electrolytes evaluated in this work.

Initially, both the porous separator and POATS-PPO showed high resistance in the coin cell leading to overpotentials exceeding 0.06 V and 0.4 V, respectively (**Figure 5**). Over the course of cycling the coin cell, the resistance decreased significantly with the overpotential of the coin cells decreasing to 0.02 V and 0.015 V, respectively (**Figure 5**). The membrane resistance and interfacial resistance can be evaluated using EIS. Comparing the Nyquist plots before and after cycling, the high frequency intercept and width of the semi-circle decrease significantly over the course of cycling (**Figure 6**), indicating that there is a decrease in both membrane and interfacial resistance during cycling. This overpotential could be caused by a thin oxidation layer on the lithium metal. Initial cycles must overcome

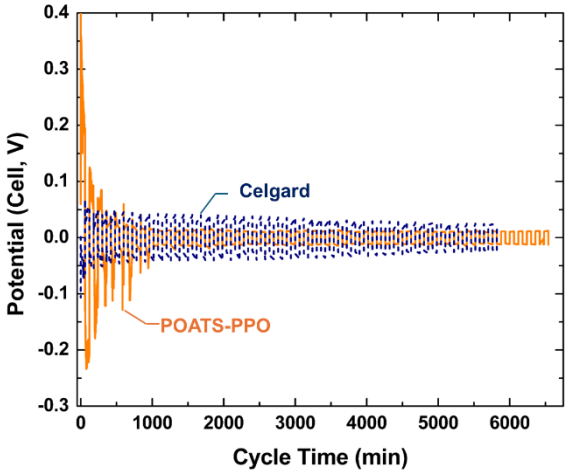

Figure 5: Constant current cycling at 0.1 mA of a lithium metal symmetric coin cell with Celgard porous membrane (dotted blue) and a POATS-PPO CEM (solid orange). Coin cells were made with lithium metal as the electrodes with 1 M LiTFSI in 3:1 DME:DOL electrolyte.

this resistive oxide layer causing an increase in cell resistance. During cycling, the oxide layer reacts away, decreasing the cell resistance leading to the steep drop in overpotential over the first 5-10 cycles.

For the POATS-PPO membrane, there is significantly more interfacial resistance than for the porous membrane. In commercial membranes, etching off membrane skin layers has been demonstrated to improve the ionic conductivity of the membrane.[29] It is

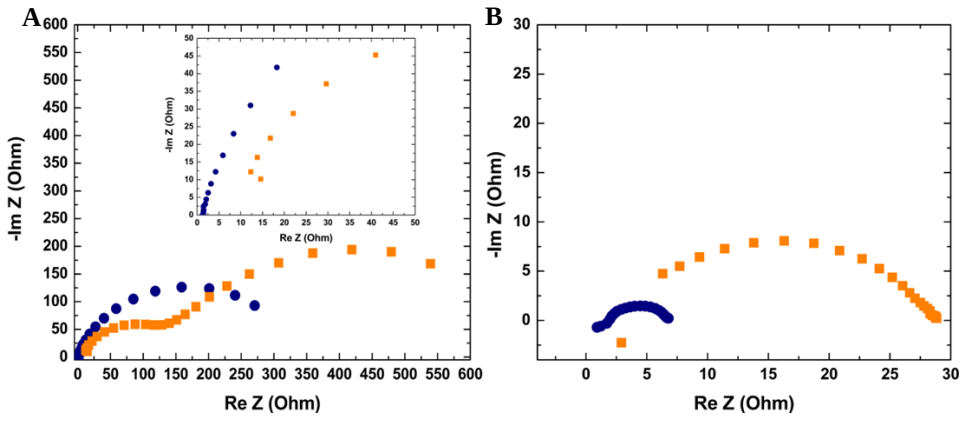

Figure 6: Nyquist plots for lithium metal symmetric coin cells from EIS measurements taken before (A, closeup inset) and after (B) cycling. Coin cells were made with lithium metal as the electrodes with 1 M LiTFSI in 3:1 DME:DOL electrolyte. Electrodes were separated by a Celgard porous membrane (●) or a POATS-PPO CEM (■).

possible that the membrane skin layer may be removed over the first few cycling by reacting with the lithium metal, decreasing the resistance of the membrane. Overall, the POATS-PPO membrane showed excellent stability over the first 100 cycles in a lithium symmetric cell with a conductivity of around 0.4 mS/cm. Because the high frequency intercept and semicircle width of the Nyquist plot both decrease with extended cycling it appears that there are no damaging side reactions that occur between the membrane and lithium metal.

Conclusions

POATS-PPO polymers were successfully synthesized and cast into membranes. Membranes were crosslinked and evaluated in TEGDME or DME:DOL solvent blends using 1 M LiTFSI as the electrolyte salt. The solvent uptake of the membranes was lowest in TEGDME also resulting in the lowest conductivity. For the blend solvents, the solvent uptake increased from 3:1 DME:DOL < 1:3 DME:DOL < 1:1 DME:DOL. It is likely that co-solvent behavior of the DME:DOL blend results in more favorable interactions between the blend solvent and the functional groups of the polymer leading to elevated solvent uptake in the 1:1 blend. Surprisingly, the conductivity was the highest in 3:1 DME:DOL, even though the solvent uptake was lower, and the electrolyte conductivity was similar to other blend solvents. This is likely caused by a skin layer which orients itself into the membrane in a solvent with more DME than DOL. POATS-PPO membranes were cycled in a lithium metal symmetric coin cell. The membrane showed stable cycling at low current density for over 100 cycles. High resistance in initial cycles may have been caused by interfacial resistance in the cell, which decrease over time resulting in improved performance after the first 10 cycles. Overall, this work demonstrates the potential for use of POATS-PPO membranes in lithium sulfur batteries based on their stability in ether-based electrolytes, promising conductivity, and stability in contact with lithium metal.

References

(1) Pathak, A. D.; Saha, S.; Bharti, V. K.; Gaikwad, M. M.; Sharma, C. S. A Review on Battery Technology for Space Application. *J. Energy Storage* **2023**, *61*, 106792. https://doi.org/10.1016/j.est.2023.106792.

(2) Zhu, J.; Zhu, P.; Yan, C.; Dong, X.; Zhang, X. Recent Progress in Polymer Materials for Advanced Lithium-Sulfur Batteries. *Prog. Polym. Sci.* **2019**, *90*, 118–163. https://doi.org/10.1016/j.progpolymsci.2018.12.002.

(3) Hepp, A.; Kumta, P.; Velikokhatnyi, O.; Datta, M. *Lithium-Sulfur Batteries: Advances in High-Energy Density Batteries*; Elsevier, 2022.

(4) Zhou, Z.; Zhao, T.; Lu, X.; Cao, H.; Zha, X.; Zhou, Z. Functionalized Polyimide Separators Enable High Performance Lithium Sulfur Batteries at Elevated Temperature. *J. Power Sources* **2018**, *396*, 542–550. https://doi.org/10.1016/j.jpowsour.2018.06.040.

(5) Salama, M.; Rosy; Attias, R.; Yemini, R.; Gofer, Y.; Aurbach, D.; Noked, M. Metal–Sulfur Batteries: Overview and Research Methods. *ACS Energy Lett.* **2019**, *4* (2), 436–446. https://doi.org/10.1021/acsenergylett.8b02212.

(6) Wujcik, K. H.; Wang, D. R.; Raghunathan, A.; Drake, M.; Pascal, T. A.; Prendergast, D.; Balsara, N. P. Lithium Polysulfide Radical Anions in Ether-Based Solvents. *J. Phys. Chem. C* **2016**, *120* (33), 18403–18410. https://doi.org/10.1021/acs.jpcc.6b04264.

(7) Barchasz, C.; Leprêtre, J.-C.; Patoux, S.; Alloin, F. Electrochemical Properties of Ether-Based Electrolytes for Lithium/Sulfur Rechargeable Batteries. *Electrochimica Acta* **2013**, *89*, 737–743. https://doi.org/10.1016/j.electacta.2012.11.001.

(8) Zhang, B.; Wu, J.; Gu, J.; Li, S.; Yan, T.; Gao, X.-P. The Fundamental Understanding of Lithium Polysulfides in Ether-Based Electrolyte for Lithium–Sulfur Batteries. *ACS Energy Lett.* **2021**, *6* (2), 537–546. https://doi.org/10.1021/acsenergylett.0c02527.

(9) Ma, G.; Huang, F.; Wen, Z.; Wang, Q.; Hong, X.; Jin, J.; Wu, X. Enhanced Performance of Lithium

Sulfur Batteries with Conductive Polymer Modified Separators. *J. Mater. Chem. A* **2016**, *4* (43), 16968–16974. https://doi.org/10.1039/C6TA07198H.
(10) Scheers, J.; Fantini, S.; Johansson, P. A Review of Electrolytes for Lithium–Sulphur Batteries. *J. Power Sources* **2014**, *255*, 204–218. https://doi.org/10.1016/j.jpowsour.2014.01.023.
(11) Kim, A.; Oh, S. H.; Adhikari, A.; Sathe, B. R.; Kumar, S.; Patel, R. Recent Advances in Modified Commercial Separators for Lithium–Sulfur Batteries. *J. Mater. Chem. A* **2023**, *11* (15), 7833–7866. https://doi.org/10.1039/D2TA09266B.
(12) Li, C.; Liu, R.; Xiao, Y.; Cao, F.; Zhang, H. Recent Progress of Separators in Lithium-Sulfur Batteries. *Energy Storage Mater.* **2021**, *40*, 439–460. https://doi.org/10.1016/j.ensm.2021.05.034.
(13) Rana, M.; Li, M.; Huang, X.; Luo, B.; Gentle, I.; Knibbe, R. Recent Advances in Separators to Mitigate Technical Challenges Associated with Re-Chargeable Lithium Sulfur Batteries. *J. Mater. Chem. A* **2019**, *7* (12), 6596–6615. https://doi.org/10.1039/C8TA12066H.
(14) Zhang, S.; Guo, W.; Yang, F.; Zheng, P.; Qiao, R.; Li, Z. Recent Progress in Polysulfide Redox-Flow Batteries. *Batter. Supercaps* **2019**, *2* (7), 627–637. https://doi.org/10.1002/batt.201900056.
(15) Karaseva, E. V.; Kuzmina, E. V.; Kolosnitsyn, D. V.; Shakirova, N. V.; Sheina, L. V.; Kolosnitsyn, V. S. The Mechanism of Effect of Support Salt Concentration in Electrolyte on Performance of Lithium-Sulfur Cells. *Electrochimica Acta* **2019**, *296*, 1102–1114. https://doi.org/10.1016/j.electacta.2018.11.019.
(16) Perry, M. L.; Saraidaridis, J. D.; Darling, R. M. Crossover Mitigation Strategies for Redox-Flow Batteries. *Curr. Opin. Electrochem.* **2020**, *21*, 311–318. https://doi.org/10.1016/j.coelec.2020.03.024.
(17) Lehmann, M. L.; Tyler, L.; Self, E. C.; Yang, G.; Nanda, J.; Saito, T. Membrane Design for Non-Aqueous Redox Flow Batteries: Current Status and Path Forward. *Chem* **2022**, *8* (6), 1611–1636. https://doi.org/10.1016/j.chempr.2022.04.005.
(18) Machado, C. A.; Brown, G. O.; Yang, R.; Hopkins, T. E.; Pribyl, J. G.; Epps, T. H. Redox Flow Battery Membranes: Improving Battery Performance by Leveraging Structure–Property Relationships. *ACS Energy Lett.* **2021**, *6* (1), 158–176. https://doi.org/10.1021/acsenergylett.0c02205.
(19) McCormack, P. M.; Luo, H.; Geise, G. M.; Koenig, G. M. Conductivity, Permeability, and Stability Properties of Chemically Tailored Poly(Phenylene Oxide) Membranes for Li+ Conductive Non-Aqueous Redox Flow Battery Separators. *J. Power Sources* **2020**, *460*, 228107. https://doi.org/10.1016/j.jpowsour.2020.228107.
(20) McCormack, P. M.; Koenig, G. M.; Geise, G. M. Transport Property Modulation via Solvent-Specific Behavior in Crosslinked Nonaqueous Membranes. *ACS Appl. Polym. Mater.* **2023**, *5* (4), 2449–2461. https://doi.org/10.1021/acsapm.2c02121.
(21) McCormack, P. M.; Koenig, G. M.; Geise, G. M. Thermodynamic Interactions as a Descriptor of Cross-Over in Nonaqueous Redox Flow Battery Membranes. *ACS Appl. Mater. Interfaces* **2021**, *13* (41), 49331–49339. https://doi.org/10.1021/acsami.1c14845.
(22) Li, Y.; Sniekers, J.; Malaquias, J. C.; Van Goethem, C.; Binnemans, K.; Fransaer, J.; Vankelecom, I. F. J. Crosslinked Anion Exchange Membranes Prepared from Poly(Phenylene Oxide) (PPO) for Non-Aqueous Redox Flow Batteries. *J. Power Sources* **2018**, *378*, 338–344. https://doi.org/10.1016/j.jpowsour.2017.12.049.
(23) Jin, K.; Torkelson, J. M. Tg and Tg Breadth of Poly(2,6-Dimethyl-1,4-Phenylene Oxide)/Polystyrene Miscible Polymer Blends Characterized by Differential Scanning Calorimetry, Ellipsometry, and Fluorescence Spectroscopy. *Polymer* **2015**, *65*, 233–242. https://doi.org/10.1016/j.polymer.2015.04.016.
(24) Leroux, C. R.; McCormack, P. M.; Elango, S.; Geise, G. M.; Koenig, G. M. Transport Properties of Ethylene Glycol Functionalized Membranes Exposed to Nonaqueous Electrolytes. *Polymer* **2024**, *300*, 126986. https://doi.org/10.1016/j.polymer.2024.126986.
(25) Petreanu, I.; Ebrasu, D.; Sisu, C.; Varlam, M. Thermal Analysis of Sulfonated Polymers Tested as Polymer Electrolyte Membrane for PEM Fuel Cells. *J. Therm. Anal. Calorim.* **2012**, *110* (1), 335–339. https://doi.org/10.1007/s10973-012-2442-z.
(26) Lufrano, F.; Gatto, I.; Staiti, P.; Antonucci, V.; Passalacqua, E. Sulfonated Polysulfone Ionomer Membranes for Fuel Cells. *Solid State Ion.* **2001**, *145* (1–4), 47–51. https://doi.org/10.1016/S0167-2738(01)00912-2.
(27) SABIC. *SABIC NORYL PPE Powder Americas Technical Data Sheet*.
(28) Kreuer, K.-D. The Role of Internal Pressure for the Hydration and Transport Properties of Ionomers and Polyelectrolytes. *Solid State Ion.* **2013**, *252*, 93–101. https://doi.org/10.1016/j.ssi.2013.04.018.
(29) Van Nguyen, T.; Vu Nguyen, M.; Nordheden, K. J.; He, W. Effect of Bulk and Surface Treatments on the Surface Ionic Activity of Nafion Membranes. *J. Electrochem. Soc.* **2007**, *154* (11), A1073. https://doi.org/10.1149/1.2781247.